INSTITUTE OF PHYSICS PUBLISHING PHYSICAL BIOLOGY
Phys. Biol. **1** (2004) 27–34 PII: S1478-3967(04)70558-6

Cooperativity can reduce stochasticity in intracellular calcium dynamics

Kai Wang, Wouter-Jan Rappel and Herbert Levine

Department of Physics and Center for Theoretical Biological Physics, University of California, San Diego, La Jolla, CA 92093-0319, USA

Received 15 October 2003
Accepted for publication 14 January 2004
Published 12 February 2004
Online at stacks.iop.org/PhysBio/1/27 (DOI: 10.1088/1478-3967/1/1/003)

Abstract
The opening of inositol (1,4,5)-triphosphate (IP_3) receptors, clustered at discrete sites on the endoplasmic reticulum, can lead to large-scale intracellular calcium waves. Recent experiments in *Xenopus* oocytes (Marchant J S and Parker I 2001 *EMBO J.* **20** 65–76) have shown that the inter-wave intervals for these waves have a standard deviation that is much smaller than their mean and that the background calcium concentration exhibits a slow rise during the interwave interval. Using a simple mathematical model, we examine the possibility that this slow rise increases the cooperativity between the openings of the clusters. We find that our model, coupled to the usual assumption that the pumps on the endoplasmic reticulum are activated instantaneously, is unable to explain the observed data: the clusters are found to fire independently and the inter-wave interval distribution is a Poisson distribution with a standard deviation that is approximately equal to its mean. On the other hand, we find that incorporating pumps that slowly activate leads to a slow increase in the background calcium concentration which makes global events progressively more likely to occur. We show that this cooperativity results in much smaller standard deviations and inter-wave interval distributions that are clearly not Poisson distributions.

1. Introduction

Ca^{2+} is an omnipresent intracellular second messenger that is involved in a wide variety of cellular functions (for a review see [1]). Its cytosolic concentration is determined by a balance of processes that bring Ca^{2+} into cytoplasm and processes that remove Ca^{2+} from the cytoplasm [10]. Ca^{2+} is brought into the cytoplasm from the extracellular space via plasma membrane transport. Additionally, Ca^{2+} can be released from intracellular stores such as the endoplasmic reticulum (ER) and sarcoplasmic reticulum (SR). Processes that reduce the cytosolic Ca^{2+} concentration include the binding of free Ca^{2+} to buffers and the removal from the cytoplasm through pumps and exchangers.

In many cell types, Ca^{2+} is released from the ER through the opening of the inositol (1,4,5)-triphosphate (IP_3) receptors (IP_3Rs). These receptors are clustered at sites [2, 3] which are positioned randomly on the ER membrane with a distance of $\sim$5–8 μm [4]. The binding of IP_3 and Ca^{2+} results in the opening of a channel which is inactivated for very high concentrations of Ca^{2+}. Through the use of novel experimental techniques that permit the visualization of subcellular events, it has become clear that Ca^{2+} dynamics can be a highly localized process. Release events, during which the IP_3Rs open and release Ca^{2+} from the ER into the cytosol, can be limited to single clusters ('puffs') or even single channels ('blips') [2, 5]. Furthermore, it has become clear that these release events exhibit a large degree of stochasticity [2, 6]. The increase in Ca^{2+} concentration due to a puff from one cluster can initiate the opening of neighboring clusters. The subsequent further increase in local Ca^{2+} concentration can then lead to a global Ca^{2+} wave.

A recent experimental study by Marchant *et al* [4] examined spontaneous global Ca^{2+} waves in immature *Xenopus* oocytes for different IP_3 concentrations. In particular, they found global waves with mean inter-wave intervals ranging from 8 s, for the highest IP_3 concentration, to 120 s for the lowest IP_3 concentration. The standard deviations for these inter-wave intervals were found to be significantly smaller than their mean and ranged from $<$2 s to $\sim$25 s. Furthermore, for the global events with large inter-wave intervals, the average cytosolic Ca^{2+} concentration was observed to increase slowly

between two waves. In contrast, the puff rate only increased during the first part of a wave cycle and then reached a sustained level.

The relatively small standard deviation observed in the experiments indicates that the puffs, which are the building blocks of the global events, are not uncoupled. After all, if the puffs were independent of the history of the system, the global events could be described by a Poisson process. Then, the distribution of mean inter-wave intervals would be exponential and the measured standard deviation should equal the measured mean inter-wave interval. Conversely, a mechanism which makes global events progressively more likely to occur as the system generates puffs would be able to explain the observed data.

In this paper, we investigate the possibility that the slow increase of the average Ca^{2+} concentration is related to the small standard deviations in the inter-wave intervals and study possible sources for this slow increase. Our basic hypothesis is that this slow rise will increase the probability that cluster openings lead to global waves. Thus, the probability of the nucleation process for a global wave will be an increasing function of time and the standard deviation will be reduced.

We address this hypothesis via the simulation of a simple computational model for Ca^{2+} dynamics. Several groups have presented detailed models of intracellular Ca^{2+} dynamics, taking into account spatial localization of the IP_3 receptor clusters [7–9]. These models have been helpful in furthering our understanding of Ca^{2+} dynamics. However, their complexity makes it difficult to investigate the essential processes involved in certain experimental observations. For this reason, we have chosen to study a very simple model, with the goal of capturing the physical mechanism that can lead to mean inter-wave intervals with small standard deviations, as caused by a slow rise in cytosolic Ca^{2+} between two successive waves. As we will see, our approach leads to the conclusion that a model consisting of a diffusive coupling between the receptor clusters, combined with *instantaneously* activated pumps on the ER is not able to explain the experimental data. Specifically, it is unable to produce both a slow cytosolic Ca^{2+} rise and a sufficient reduction in cytosolic Ca^{2+} after a global event. Thus, our model needs to incorporate an additional mechanism and we show that incorporating a pump which slowly activates is one possible way to account for the experimental findings.

2. The Ca^{2+} model

The basic elements of Ca^{2+} dynamics include diffusion through the cytosol, release from the ER through IP_3Rs and the uptake into ER through SERCA pumps. Thus, we start with the reaction–diffusion equation

$$\frac{\partial[Ca^{2+}]}{\partial t} = J_{\text{release}} - J_{\text{uptake}} + D\nabla^2[Ca^{2+}] \tag{1}$$

where D is the Ca^{2+} diffusion constant. We have chosen a two-dimensional $150 \times 150\ \mu$m square computational domain with zero-flux boundary conditions and a spatial discretization of 0.5 μm; this is large enough to study large-scale calcium dynamics. The first term of this equation models the release of Ca^{2+} from the IP_3Rs. Instead of using a detailed channel model as in previous studies [10–13], we use a simple point-source description which reads

$$J_{\text{release}} = \nu_r \sum_{i,j} \delta(\vec{x} - \vec{x}_i)\delta\left(t - t_i^j\right) \tag{2}$$

where $\vec{x}_i$ is the position of a cluster site, and t_i^j gives the time of the jth puff at site $\vec{x}_i$. (see also [14]). The cluster sites are located on a square grid with a grid spacing of $d = 6\ \mu$m. During each puff a constant amount of Ca^{2+} is released instantaneously. Estimated from experiments [2], the amount is chosen here as $\nu_r = 70\,\mu\text{M}\ \mu\text{m}^{-2}$.

Stochasticity is built in the model via the description of the 'firing' times t_i^j. To this end, we associate with each cluster site a stochastic controlling variable θ and generate a puff at that site when the value of this variable exceeds a threshold, θ_{th}. The fact that the firing is controlled by Ca^{2+} (the well-known CICR mechanism [5]), is incorporated by making this threshold a function of the Ca^{2+} concentration. In general we expect this dependence to be sigmoidal, corresponding to a high, baseline threshold at low concentration dropping to a low threshold at high concentration. Here we take the simplest caricature,

$$\begin{aligned} \theta_{\text{th}} &= \theta_{\text{th},0} \qquad \text{for} \quad Ca^{2+} < Ca^{2+}_{\text{th}} \\ \theta_{\text{th}} &= -\infty \qquad \text{for} \quad Ca^{2+} \geqslant Ca^{2+}_{\text{th}}. \end{aligned} \tag{3}$$

In other words, for Ca^{2+} levels exceeding Ca^{2+}_{th} the threshold becomes infinitely low and the cluster will fire with probability 1, which will be called a triggered puff. For Ca^{2+} levels below Ca^{2+}_{th} the cluster will only release Ca^{2+} when θ exceeds $\theta_{\text{th},0}$, which will be called a spontaneous puff. To incorporate a refractory period we specify that after a threshold crossing θ is reset to 0 where it remains for a fixed period of time. The equation for θ reads:

$$\text{d}\theta = -\Gamma\theta\,\text{d}t + \sigma\,\text{d}W \tag{4}$$

where W is a standard Wiener process and where the positive Γ ensures a stochastic process centered around 0. In the following, we have fixed $\theta_{\text{th},0} = 1.05, \Gamma = 1\ \text{s}^{-1}$, and $\sigma = 0.2\ \text{s}^{-1/2}$. The refractory period is set to 7 s, following the minimum period seen in Parker's data [4]. We will vary the Ca^{2+} threshold to mimic the effect of varying IP_3 in the experiments.

The second term in our equation describes the uptake of the cytosolic Ca^{2+} into the ER via the SERCA pumps. We assume that the pumps are uniformly distributed on the ER membrane and that the uptake can be described by

$$J_{\text{uptake}} = r_u[Ca^{2+}]. \tag{5}$$

As we will discuss below, the exact form of the pumping rate r_u might play a determining role in the distribution of inter-wave intervals. We will assume here that r_u obeys a first-order reaction

$$\tau_u \frac{\partial r_u}{\partial t} = \nu_u[Ca^{2+}]^2 - \left([Ca^{2+}]^2 + K_u^2\right)r_u. \tag{6}$$

The parameter τ_u controls the time scale of the pump kinetics and we will consider two cases. The first one, customarily used

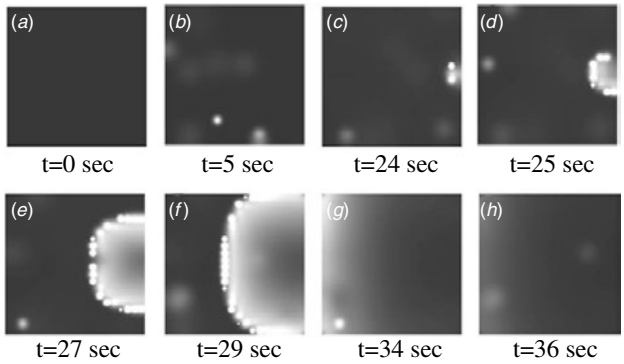

Figure 1. Snapshots of calcium puffs and a global calcium wave simulated by the model with ultra-fast SERCA kinetics within a 150×150 μm region and with $[Ca^{2+}]_{th} = 0.095$ μM. After many stochastic puffs, a global wave is initiated from the right side of the region and spreads over the whole region in about 10 s. Here, and in the remainder of the figures, the parameter values are: $\nu_r = 70$ μM μm^{-2}, $\theta_{th,0} = 1.05$, $\Gamma = 1$ s^{-1}, $\sigma = 0.2$ s$^{-1/2}$, $\nu_u = 0.5$ μM s^{-1}, $K_u = 0.31$ μM and $D = 25$ μm^2 s^{-1}.

in modeling studies and which we will call ultra-fast SERCA kinetics, is the limit of small τ_u. In this case, r_u reaches equilibrium very quickly and J_{uptake} can be described by $J_{uptake} = \nu_u[Ca^{2+}]^2/([Ca^{2+}]^2 + K_u^2)$. This Hill function form of J_{uptake} has been seen experimentally and we have chosen the values of the parameters to be consistent with measured data [15–17] and theoretical models [7, 18]: $\nu_u = 0.5$ μM s^{-1}, and $K_u = 0.31$ μM. The second case investigated here corresponds to taking a non-zero value of τ_u. In this case, we can no longer use the steady-state solution for r_u, which now has to be solved explicitly through equation (6). We will call this case slow SERCA kinetics and we have chosen $\tau_u = 1.25$ s.

The last term in our equation describes the diffusion of free Ca^{2+}. In reality, most of the cytosolic calcium is bound by calcium buffer proteins. Generally, the buffers are present in large concentrations and have fast binding kinetics relative to the time scale of global calcium waves. Therefore, we assume that the buffers are always in equilibrium with free Ca^{2+}. This assumption can be shown to result in a simple renormalization of the diffusion constant which we take $D = 25$ μm^2 s^{-1}, a value that falls within the experimentally observed range [19].

3. Results

3.1. Ultra-fast SERCA kinetics

We start by showing in figure 1 several typical snapshots of the Ca^{2+} concentration field as simulated by the model with ultra-fast SERCA kinetics. These snapshots are qualitatively similar to those using slow SERCA kinetics (data not shown). The Ca^{2+} concentration is shown on a gray scale with white corresponding to high and black corresponding to low Ca^{2+} concentrations. Initially there is no activity in the entire region, as we start our simulation with all θ's set to zero and with a uniform zero Ca^{2+} concentration (figure 1(a)). Gradually, some stochastic puffs appear, as shown by the small white circles in figure 1(b). These puffs can then trigger neighboring cluster sites to open (right side in figure 1(c)), which releases more Ca^{2+}. This, in turn, will trigger more neighboring sites to open (figure 1(d)) and a global calcium wave is initiated (figure 1(e), (f)). This wave was found to propagate with a wave speed of approximately 15 μm s^{-1}, which falls into the measured velocity region [20, 21]. After the wave has swept through the entire computational domain (figure 1(g)), almost all the puff sites have been triggered and thereby entered the refractory period (figure 1(h)). During this refractory period, no puffs are generated while Ca^{2+} is continuously pumped back into ER by the SERCA pumps. After the refractory period, a new cycle can begin.

Figure 2 shows a full simulation run for ultra-fast SERCA kinetics. The calcium concentration shown in figure 2(a) is an average over the whole computational domain. Unlike the experiments, it is obviously very irregular. In figure 3 we show the mean of the inter-wave intervals, along with its standard deviation, as a function of $[Ca^{2+}]_{th}$. Each simulation was run for a sufficiently long time so that at least 100 global waves were counted. As in the experiments, the mean increases from 10 s, close to the refractory period, to 100 s as the Ca^{2+} threshold, which is inversely related to the IP_3 concentration, is increased. As seen, the standard deviation is roughly equal to the mean of the inter-wave interval plus the refractory period, which is much larger than the one observed in the experiments. This indicates that the global waves are uncoupled and can be described by a Poisson process (supplemented by a refractory period). This is further illustrated by figure 4 where we plot the distribution of inter-wave intervals for the simulation shown in figure 2. As demonstrated by the solid line, which is obtained through a two-parameter fit $A\exp(-(T-7)/(T_0-7)$, the distribution is well described by an exponential, a hallmark of the Poisson process.

As mentioned above, our basic hypothesis is that the slow rise in background Ca^{2+} is important in limiting the variance. Our model so far is consistent with this claim which is shown in figure 2(b), where we plot the background Ca^{2+} concentration as a function of wave phase between two global waves. The background concentration was measured by averaging the concentration over the whole simulated region and over 250 different inter-wave intervals. Contrary to the experiments, the simulations show no discernible rise in the background Ca^{2+} concentration. It is therefore not surprising that the global waves are completely Poissonian. Finally, for completeness we show in figure 2(c) the corresponding puff rate, defined as the average number of puffs per second. The puff rate following a global wave increases during the first 1/5 wave cycle and then reaches a steady-state level until another global wave occurs.

Let us now address why the ultra-fast kinetics fails to describe the experimental findings. For ultra-fast kinetics, the Ca^{2+} released in a puff will be pumped backed into the ER very quickly. This is illustrated in figure 5(a) where we have plotted as a dashed line the global background Ca^{2+} concentration as a function of time after a single puff (at $t = 0$ s) for the case of ultra-fast kinetics. The Ca^{2+} concentration reaches an almost constant level very quickly after the release. Thus, unless the

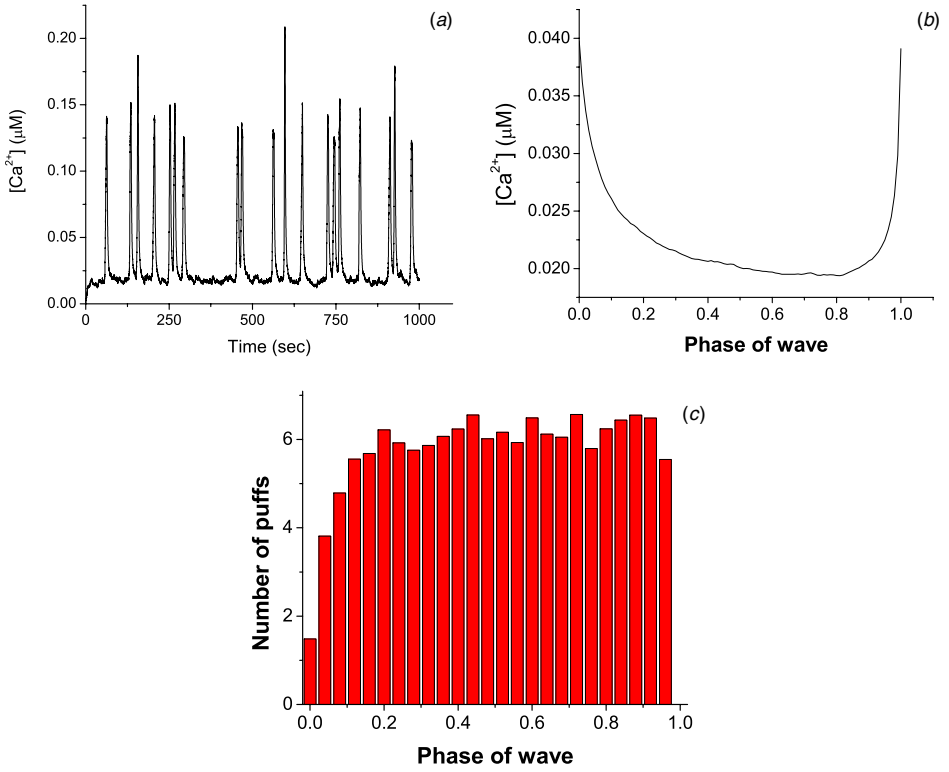

Figure 2. Cytosolic calcium concentration exhibits irregular global oscillations for the case of ultra-fast SERCA kinetics with $[Ca^{2+}]_{th} = 0.1\ \mu M$. (*a*) A trace of $[Ca^{2+}]$ for the first 1000 s. (*b*) Cytosolic calcium level averaged over 250 interwave intervals as a function of a rescaled wave phase beginning immediately after a global wave. (*c*) Corresponding averaged puff frequency as a function of wave phase.

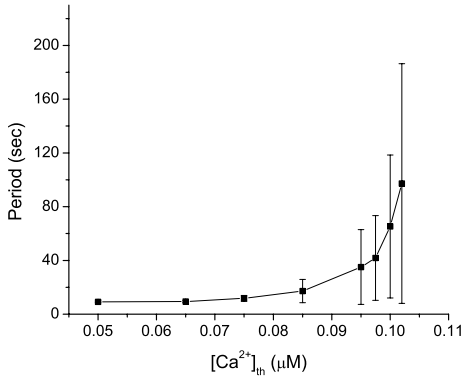

Figure 3. The mean and standard deviation of inter-wave intervals as a function of $[Ca^{2+}]_{th}$ for the model with ultra-fast SERCA kinetics.

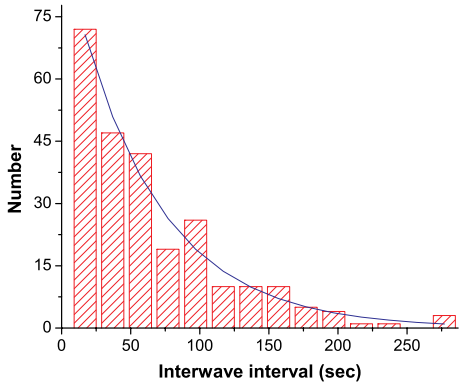

Figure 4. The distribution of inter-wave intervals for the ultra-fast SERCA kinetics case and $[Ca^{2+}]_{th} = 0.1\ \mu M$. The mean inter-wave interval for this distribution is 65.3 s while the standard deviation is 53.2 s. It fits well to an exponential distribution $A \exp(-(T-7)/(T_0-7))$. The value of the fitting parameters are $A = 0.0168\ s^{-1}$ and $T_0 = 67.9$ s.

pump rate is very low, the Ca^{2+} is prevented from diffusing far from the release site (see figure 5(*b*)) and the global background Ca^{2+} will not exhibit a slow increase over time. Consequently, the puff sites will always fire independently and the probability for a global event remains constant over time.

One obvious way to prevent the Ca^{2+} from being pumped back into the ER is to reduce the pump rate via the reduction of v_u. However, reducing this rate also reduces the ability of the pumps to reduce the Ca^{2+} concentration after a global event. We found, through extensive numerical experiments, that reducing the value of v_u results in Ca^{2+} concentrations that are above or very close to the Ca^{2+} threshold after a global event. Thus, this reduction was always accompanied by a significant decrease in the inter-wave interval. One could not get long inter-wave intervals together with weak pumping. Thus, a new mechanism is needed.

3.2. Slow SERCA kinetics

A possible mechanism that will permit large inter-wave intervals coupled with background Ca^{2+} concentrations that

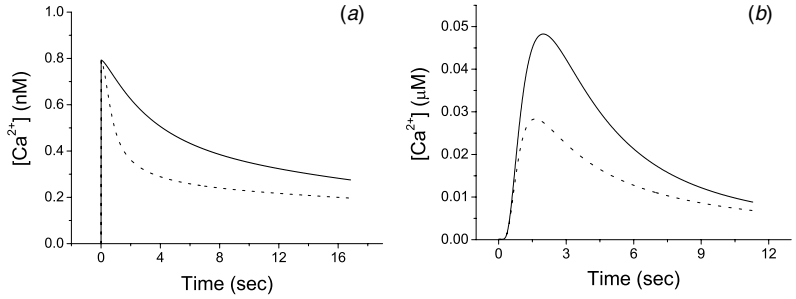

Figure 5. (*a*) Global $[Ca^{2+}]$ (measured as an average over the whole computational domain) as a function of time after a single puff at $t = 0$ for ultra-fast SERCA kinetics (dashed line) and slow SERCA kinetics (solid line). (*b*) $[Ca^{2+}]$ at a cluster site neighboring a single puff release site for ultra-fast (dashed line) and slow SERCA kinetics (solid line).

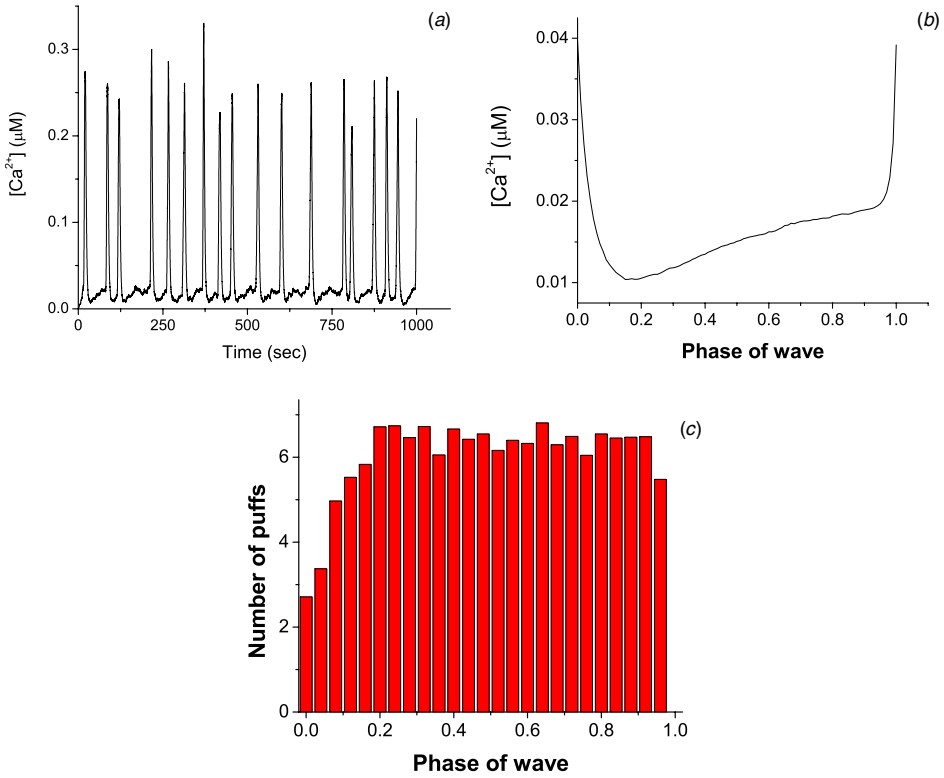

Figure 6. Cytosolic calcium concentration exhibits periodical global oscillation in the case of slow SERCA kinetics with $[Ca^{2+}]_{th} = 0.12\ \mu$M. (*a*) A trace of $[Ca^{2+}]$ for the first 1000 s. (*b*) Cytosolic calcium level averaged over 172 interwave intervals as a function of a rescaled wave phase beginning immediately following a global wave. (*c*) Corresponding averaged puff frequency as a function of wave phase.

accumulate slowly between global events is the inclusion of slow SERCA kinetics. The slow kinetics ensures that after a release event, the pump activity is initially not very high and the released Ca^{2+} can diffuse away from the cluster site. This leads to a slow build-up of background Ca^{2+}, which reduces the threshold for firing and which leads to global waves with a large mean and a small standard deviation. On the other hand, by choosing the time scale of the kinetics to be smaller than the refractory period, the pumps are still able to efficiently bring the Ca^{2+} concentration to small levels after a global event.

To verify this qualitative picture, we have performed a series of numerical simulations. Figure 6(*a*) shows a sample simulation of slow SERCA kinetics with roughly the same mean inter-wave interval as in figure 2. But in this simulation, global waves are much more regular compared to the case of ultra fast kinetics, and each global wave is indeed preceded by a slow background increase. Furthermore, in figure 7 we show the mean of the inter-wave intervals and its standard deviation as a function of $[Ca^{2+}]_{th}$. As in the case of ultra-fast kinetics, the mean inter-wave intervals ranges from 10 s to 90 s but now the standard deviation is much smaller and comparable to the experimental one. In figure 8 we show the distribution of inter-wave intervals based on 172 global events. The inter-wave interval is clearly not exponentially distributed and thus the global wave generation can no longer be described by a Poisson process.

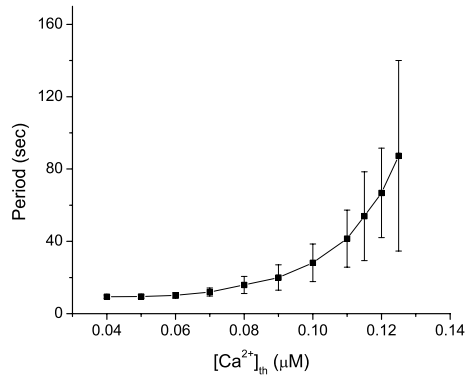

Figure 7. The mean and standard deviation of inter-wave intervals as a function of $[Ca^{2+}]_{th}$ for the model with slow SERCA kinetics.

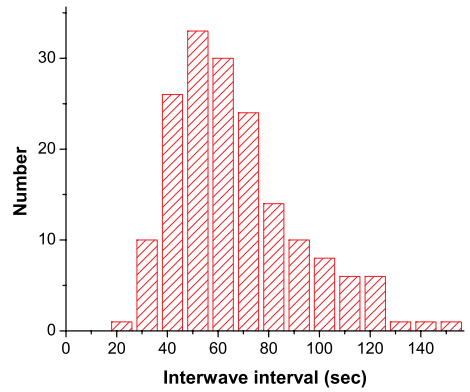

Figure 8. The distribution of inter-wave intervals for the slow SERCA kinetics case and $[Ca^{2+}]_{th} = 0.12\ \mu$M. The mean inter-wave interval for this distribution is 66.8 s while the standard deviation is 24.7 s.

Our hypothesis claims that the probability for the occurrence of a global event depends on the background Ca^{2+} concentration. In figure 6(b) we plot the background Ca^{2+} concentration, again measured by averaging $[Ca^{2+}]$ over the whole simulated region and over 172 global events. As in the experiment, the background Ca^{2+} concentration rises slowly by about 0.01 μM between two global events. This cumulative increase of Ca^{2+} should lead to an increased wave nucleation probability. It is important to note, though, that, as in the experiments, the simulated puff rate (shown in figure 6(c)) does not change significantly during the latter parts of the wave cycle. This is because most of the puffs are spontaneous and independent of each other. However, during a nucleation process, all the involved puffs are correlated via the Ca^{2+} concentration. Therefore, the distribution of the 'triggered puffs' should be a proper measure of the effect of the background Ca^{2+} level. To measure this distribution in our simulations, we labeled an event a triggered puff when the calcium concentration exceeded $[Ca^{2+}]_{th}$. Furthermore, since we are interested in the effect of calcium accumulation, we only considered the puff that triggered the global wave. In figure 9 we show the distribution of triggered events for both cases. The distribution shown here is confined by the distribution of global waves because we cannot measure the appearance times of triggered puffs which are longer than the intervals of global waves. The distribution for ultra-fast SERCA kinetics shows that nucleation processes are likely to occur during both the early and late stages of an interwave interval. In contrast, figure 9(b) demonstrates that the nucleation probability for slow SERCA kinetics is an increasing function of time and is vanishingly small immediately following a global event.

To further elucidate the contribution of slow SERCA kinetics to the background Ca^{2+} increase, we have plotted in figure 5(a) as a solid line the global Ca^{2+} concentration as a function of time after a single puff for the case of slow kinetics. Contrary to the case of ultra-fast kinetics (dashed line), the Ca^{2+} concentration decays slowly. In figure 5(b) we plot the Ca^{2+} concentration as a function of time at the cluster site that neighbors a site from which Ca^{2+} is released at $t = 0$ s. As expected, slow SERCA kinetics (solid line) results in a much higher Ca^{2+} concentration in the cytoplasm during a puff than does ultra-fast kinetics (dashed line).

4. Discussion

Our results are two-fold. First, we show that a new mechanism is needed to account for the slow rise in global Ca^{2+} during the inter-wave period. We propose that a simple possibility is afforded by relaxing the usual assumption of instantaneous SERCA pump activation. The detailed kinetics of the pumps have been measured for both SERCA1 [22, 23] and for SERCA3 [24]. An estimate based on kinetic parameters of SERCA1 shows that the typical time scale for the pump to reach a new equilibrium working state upon a rapid change in the cytosolic Ca^{2+} concentration is about 0.1 s, which is much smaller than we postulated in our model. However, the major isoform of SERCA in Xenopus oocytes is SERCA2b, which is proving to be very different from the other isoforms due to its higher sensitivity to calcium and slower turnover rate [16, 25]. Moreover, a very recent study on the kinetics of SERCA2b shows that some of the reaction steps of SERCA2b are much slower than their counterparts in SERCA1 and SERCA3 [26]. On the other hand, recent experimental data on the dynamics of cytosolic calcium following influx of extracellular calcium suggests that there is no lag in the activation of the SERCA pumps [27]. It is probably fair to say that more work is needed to definitively prove or disprove the possibility of slow pump kinetics.

The second result concerns the necessity and sufficiency of the slow Ca^{2+} rise in limiting the variance of the inter-wave interval. The sufficiency is clear, but the question is whether this is the only possible mechanism is more complicated. After all, this necessity has been shown in a model which is rather simple and in particular ignores the detailed biochemistry involved in the channel dynamics. We have verified that relaxing some of the simplifying assumptions in our model (such as the all-or-none nature of the puff) do not alter any of our conclusions, but it is hard to check all possible modifications. In the work of Falcke [8], who studied global oscillations using the deYoung–Keizer kinetics [11], there is some limitation in the variance as compared to the mean due to what appears to be an effective increase in the refractory

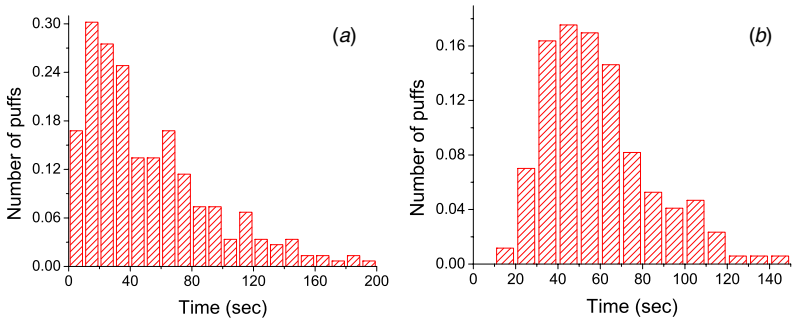

Figure 9. The distribution of triggered puffs for ultra-fast SERCA kinetics with $[Ca^{2+}]_{th} = 0.1\ \mu M$ (*a*) and slow SERCA kinetics with $[Ca^{2+}]_{th} = 0.12\ \mu M$ (*b*). In (*a*), the distribution was obtained by examining 149 global waves, containing 251 puffs, while in (*b*), the distribution was found by simulating 172 global waves with 172 puffs.

period as IP_3 is lowered. His simulations do not show the slow background rise and therefore the interval distribution presumably remains exponential after the refractory period. It should therefore be straightforward in principle to distinguish the single-puff biochemical effects as seen in his work from the inter-puff coordination effects seen in our model.

Our model suggests several new directions for experiments. First, it is clear that the most important diagnostic of the global wave nucleation mechanism is the interval distribution function. Different models lead to very different distributions, which offers a way to examine their validity in experiments. Next, we predict that altering SERCA kinetics either pharmacologically or genetically would lead to changes in global oscillation behavior—faster pumps mean more randomness in the oscillations and less Ca^{2+} accumulation. Finally, measuring the spatial correlations among puff sites (our notion of the 'triggered' as opposed to 'spontaneous' puff) should reveal how global waves are organized from their fundamental constituents.

It is clear that our modeling efforts are only a first step towards understanding cooperativity in Ca^{2+} release events and that there is room for extensions. Most notably, we have restricted ourselves to two dimensions, while the actual cell is, of course, three dimensional. It is possible that adding a third dimension will alter the Ca^{2+} dynamics. Specifically, Ca^{2+} released by a puff can now diffuse away from the ER and some of the Ca^{2+} will 'escape' from the SERCA pumps. This escape could have the same effect as our proposed delay of the pump activation. To incorporate the third dimension, however, is computationally challenging and is further complicated by the possible effects of buffers. These buffers come in different forms, including mobile and stationary, and fast and slow and their kinetics can have a profound effect on the Ca^{2+} dynamics [27].

Cooperative and stochastic events are not limited to Ca^{2+} dynamics in *Xenopus* oocytes. For example, recent experimental work suggests that cooperativity might play a role in Ca^{2+} dynamics in myocytes [28]. In these cells, Ca^{2+} functions as the key substance in the excitation-contraction coupling and enters the cell through voltage gated channels [29]. The Ca^{2+} concentration is further increased via the opening of ryanodine-sensitive channels on the SR (CICR). These channels are clustered in a nearly crystalline array and the opening of one cluster leads to a local Ca^{2+} release event, called a 'spark' in the myocyte-literature.

The response to activation is graded, meaning that SR Ca^{2+} release is proportional to the amount of Ca^{2+} that enters the cell through voltage gated channels. This gradedness is crucial in ensuring a proper function of the excitation–contraction coupling machinery, failure of which can have dire consequences [30, 31]. It requires a mechanism that can terminate a spark and prevent an 'all-or-none' response. One such mechanism could involve coupled gating, during which several channels display synchronized openings and closings [28]. In addition to this cooperative mechanism, other factors might play an important role in the termination of the sparks. These include the complicated geometry of the cardiac cell and the stochasticity due to the small numbers of calcium ions involved in the CICR process [32].

Although building and studying models that incorporate these processes is challenging, the potential rewards are significant. Several groups, including ours, are currently working towards implementing algorithms that can faithfully describe stochastic Ca^{2+} dynamics in complex three-dimensions.

Acknowledgments

We acknowledge useful discussions with M Falcke and I Parker. This work has been supported in part by the NSF-sponsored Center for Theoretical Biological Physics (grant numbers PHY-0216576 and 0225630).

References

[1] Berridge M J, Bootman M D and Roderick H L 2003 *Nat. Rev. Mol. Cell Biol.* **4** 517–29
[2] Sun X P, Callamaras N, Marchant J S and Parker I 1998 *J. Physiol.* **509** 67–80
[3] Mak D, McBride V, Raghuram Y, Joseph S and Foskett J 2000 *J. Gen. Physiol.* **115** 241–55
[4] Marchant J S and Parker I 2001 *EMBO J.* **20** 65–76
[5] Bootman M D, Lipp P and Berridge M J 2001 *J. Cell Sci.* **114** 2213–22
[6] Bootman M D, Berridge M J and Lipp P 1997 *Cell* **91** 367–73
[7] Shuai J W and Jung P 2003 *Proc. Natl Acad. Sci. USA* **100** 506–10
[8] Falcke M 2003 *Biophys. J.* **84** 42–56

[9] Falcke M 2003 *Biophys. J.* **84** 28–41
[10] Schuster S, Marhl M and Höfer T 2002 *Eur. J. Biochem.* **269** 1333–55
[11] DeYoung G W and Keizer J 1992 *Proc. Natl Acad. Sci. USA* **89** 9895–9
[12] Li Y and Rinzel J 1994 *J. Theor. Biol.* **166** 461–73
[13] Swillens S, Dupont G, Combettes L and Champeil P 1999 *Proc. Natl Acad. Sci. USA* **96** 13750–5
[14] Coombes S and Timofeeva Y 2003 *Phys. Rev.* E **68** 021915
[15] Camello P, Gardner J, Petersen O H and Tepikin A V 1996 *J. Physiol.* **490** 585–93
[16] Lytton J, Westlin M, Burk S E, Shull G E and MacLennan D H 1992 *J. Biol. Chem.* **267** 14483–9
[17] Ji Y, Loukianov E and Periasamy M 1999 *Anal. Biochem.* **269** 236–44
[18] Shuai J W and Jung P 2002 *Biophys. J.* **83** 87–97
[19] Albritton N L, Meyer T and Streyer L 1992 *Science* **258** 1812–5
[20] Marchant J, Callamaras N and Parker I 1999 *EMBO J.* **18** 5285–99
[21] John L M, Lechleiter J D and Camacho P 1998 *J. Cell Biol.* **142** 963–73
[22] Inesi G, Kurzmack M and Lewis D 1988 *Methods Enzymol.* **157** 154–90
[23] Sumbilla C, Lewis D, Hammerschmidt T and Inesi G 2002 *J. Biol. Chem.* **277** 13900–6
[24] Dode L, Vilsen B, Baelen K V, Wuytack F, Clausen D and Andersen J P 2002 *J. Biol. Chem.* **227** 45579–91
[25] Verboomen H, Wuytack F, Van Den Bosch L, Mertens L and Casteels R 1994 *Biochem. J.* **302** 979–84
[26] Dode L, Andersen J P, Leslie N, Dhitavat J, Vilsen B and Hovnanian A 2003 *J. Biol. Chem.* **278** 47877–89
[27] Dargan S L and Parker I 2003 *J. Physiol.* **553** 775–88
[28] Marx S O, Gaburjakova J, Gaburjakova M, Henrikson C, Ondrias K and Marks A R 2001 *Circ. Res.* **88** 1151–8
[29] Bers D M 2001 *Excitation-Contraction Coupling and Cardiac Contractile Force* (Boston, MA: Kluwer)
[30] Gomez A M, Valdivia H H, Cheng H, Lederer M R, Santana L F, Cannell M B, McCune S A, Altschuld R A and Lederer W J 1997 *Science* **276** 800–806
[31] Pogwidz S M and Bers D M 2002 *J. Cardiovasc. Electrophysiol.* **13** 88–91
[32] Irvine L A, Jafri M S and Winslow R L 1999 *Biophys. J.* **76** 1868–85